COMBINED THEORY AND EXPERIMENTAL VERIFICATION OF PLASTRON STABILITY ON SUPERHYDROPHOBIC SURFACE

Ning Yu, Zhaohui "Ray" Li, Alexander McClelland, and Chang-Jin "CJ" Kim
University of California, Los Angeles, CA, USA

ABSTRACT

This paper (i) develops a theoretical model to predict the fate of plastron, or the air pockets on superhydrophobic (SHPo) surface under water, in high-speed flows and (ii) assess the developed model experimentally by testing a range of well-defined microtrench SHPo surfaces attached underneath a motorboat on seawater. The comprehensive model, which addresses all the important factors that affect the plastron and its drag-reducing ability in flowing water, has long been desired but missing to design SHPo surfaces for underwater applications over a range of flow conditions including a real marine environment.

KEYWORDS

Superhydrophobic surface, Plastron stability

INTRODUCTION

Superhydrophobic (SHPo) surfaces have been a popular topic for more than two decades. For most important applications, the SHPo surfaces are completely immersed under a liquid (predominantly water), making the existence of plastron the most critical issue. Unfortunately, however, the state of plastron has too often been ignored due to the difficulty of observing and addressing it during the main experiments for applications. Among the applications, drag reduction of watercraft has been the most frequently cited for its global impact on energy saving and environmental protection. Yet, a successful drag reduction under fully turbulent flows in real marine conditions was reported only recently [1], because the plastron is easily depleted under such severe conditions. Several factors that affect the plastron have been identified and studied over the years: hydrostatic pressure and air diffusion [2], shear drainage [3], surfactant [4], etc. Concluding that all the important factors have now been identified, here we develop a comprehensive model that can predict the plastron stability and guide the design of SHPo surfaces for a given application.

THEORY

Consider a SHPo surface immersed under water. When the pressure difference across the air-water interface (i.e., meniscus), i.e., $\Delta P = P_{water} - P_{air}$, reaches the maximum Laplace the interfacial tension can provide, the meniscus will start depinning from the top edges of asperities either into or out of the surface, as shown in Figure 1(a) or Figure 1(b), respectively, deteriorating the drag-reduction ability of the SHPo surface. The range of pinning the Laplace pressure can provide depends on the material hydrophobicity and asperity geometries, as follows:

$$\Delta P_i = -\sigma/R_i = -2\sigma\cos\theta_{dp\text{-}i}/w \quad (1)$$

$$\Delta P_o = -\sigma/R_o = -2\sigma\sin\theta_{dp\text{-}o}/w \quad (2)$$

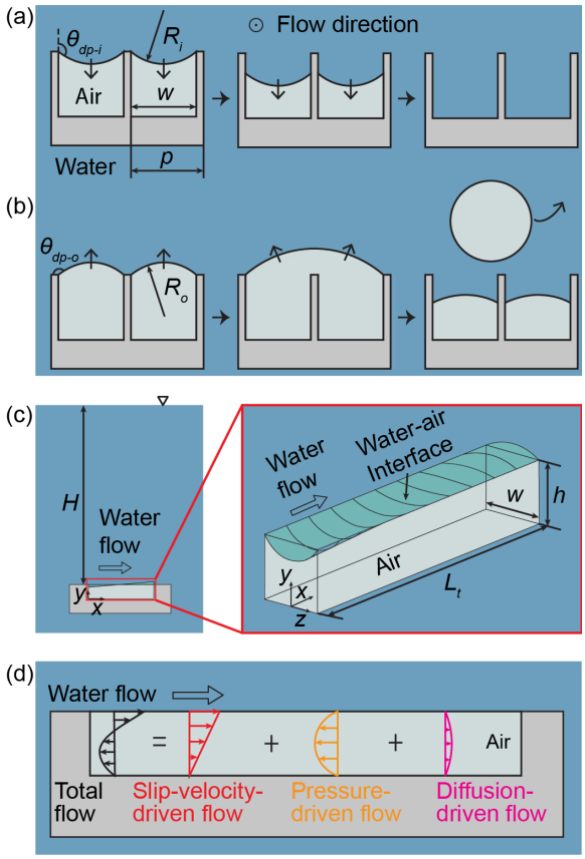

Figure 1: Theoretical analysis. (a) Water-air interface depins into trench. (b) Water-air interface depins out of trench. (c) Plastron morphology in a trench under water flow. (d) Velocity profile of plastron, i.e., the trapped air, inside a microtrench.

where the subscript *i* and *o* represent inward and outward, correspondingly. R_i and R_o are the minimum radii of the meniscus on each curving direction, as shown in Figure 1(a)(b), σ is the surface tension of water, and w is the trench width. Usually, $\theta_{dp\text{-}i}$ equals the advancing contact angle of water on the hydrophobic coating. However, the SHPo surface with re-entrant edges expands the range to $\theta_{dp\text{-}i} = 180°$ [1]. On the other hand, usually $\theta_{dp\text{-}o}$ equals the receding contact angle on the hydrophobic coating, but SHPo surface with the Salvinia effect may expand the range to $\theta_{dp\text{-}o} = 90°$ [5].

A well-known factor for plastron stability is the air diffusion across the interface by hydrostatic pressure [2]. Applying the recently reported theory of oil stability on liquid infused surface (LIS) [3] to SHPo surfaces, we can identify another factor for the plastron stability – air drainage by the shear stress of high-speed flows. Combining the above two theories, in this paper we develop a unified model, leading to Figures 1(c) and 1(d), which present the shape of the pinned meniscus and the flow profile of the trapped air, respectively.

EXPERIMENTAL SETUP

For experiments, we fabricated a series of 4x7 cm^2 SHPo surfaces with various pitches (p), widths (w), depths (h), and lengths (L_t) of trenches from 4" silicon wafers, using photolithography, deep reactive ion etching (DRIE), sample dicing, and vapor-based perfluorodecyltrichlorosilane (FDTS) coating. The pictures of a sample are shown in Figure 2(a). The SEM pictures show that there is a ~250 nm undercut below the silicon dioxide layer at the top, making edges of trenches re-entrant. Using an instrument custom-built in our lab, the advancing and receding contact angle of water on FDTS-coated smooth silicon surface were measured to be 116±2° and 101±1°. The micro trenches on the sample have two types of pitches, p = 75 and 100 µm, and a uniform gas fraction, w/p = 0.9. For each pitch, various trench lengths (i.e., L_t = 2.5, 5, 10, 30, 60 mm) were made by adding spanwise segments in the trench, as shown in Figure 2(b). Two trench depths were fabricated, h = 50, 90 µm, by using two wafers. The smooth area between the SHPo region and the sample edge is to prevent the effect of the space gap between the sample and the surrounding surface on the wetting.

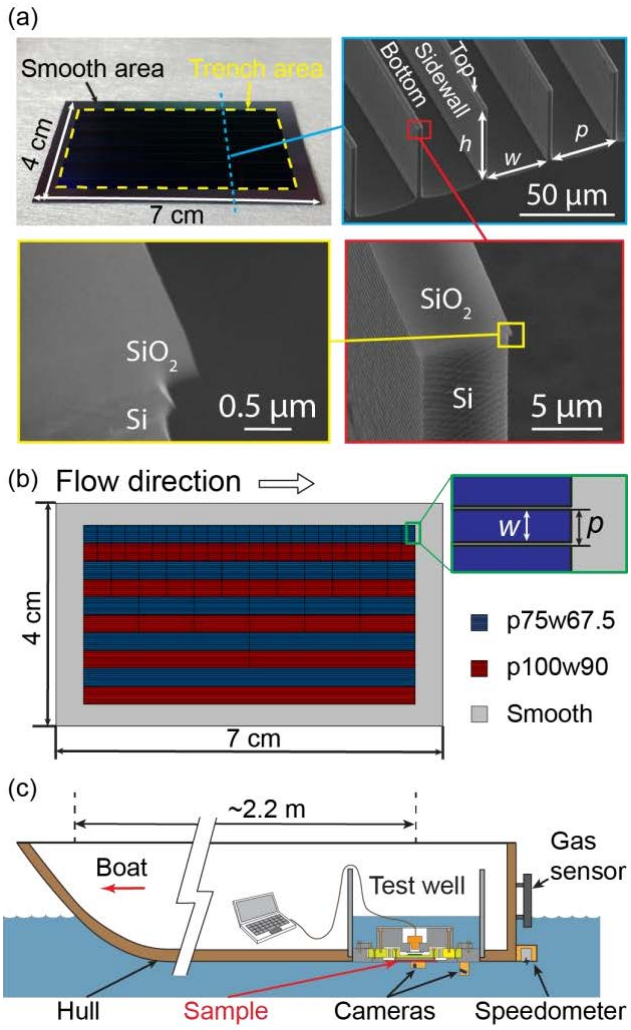

Figure 2: Sample fabrication and experimental setup. (a) Sample pictures. The insect SEM image with cyan frame shows the cross-section of trenches cleaved along the cyan dotted line. Zoom-in SEM pictures with red and yellow frames show the re-entrant structure on the trench top. (b) Schematic illustration of the parallel-trench SHPo surface with various trench widths and lengths. Blue segments have p = 75 µm, w = 67.5 µm; red segments have p = 100 µm, w = 90 µm. (c) Schematic cross-section of the retrofitted boat. The SHPo sample is attached underneath, replacing a part of the boat hull.

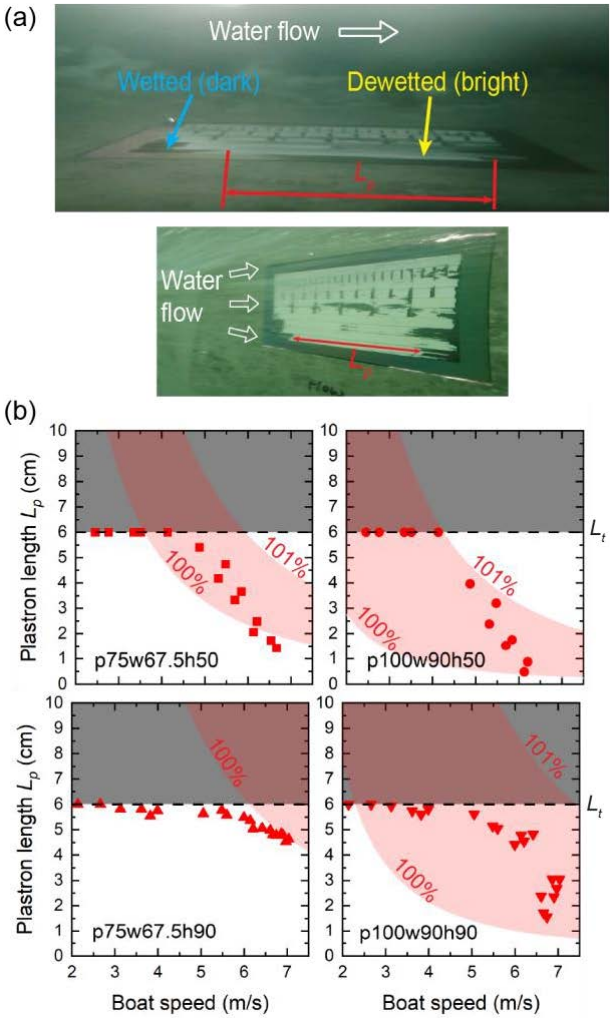

Figure 3: Experimental results. (a) Underwater sample images at high-speed water flow (~5.7 m/s). The top and bottom images are from the side and back camera, respectively. The length of plastron is labeled by the red arrows. (b) Experimental data (red symbols) of plastron length, L_p vs. boat speed, compared with the theoretical prediction (red shade). The top two graphs are for h = 50 µm, and the bottom two graphs are for h = 90 µm. The plastron length is the average value of L_p measured on 6 cm-long trenches of 4 different samples in water with air saturation levels between 100% and 101%. While L_p can be larger than 6 cm mathematically (grey shade), experimentally it is limited to 6 cm, which is the length of the longest trench on the current samples.

The SHPo surfaces were attached at the bottom of a motorboat and observed using two underwater cameras, as shown in Figure 2(c). The two cameras were positioned to view the plastron in two orthogonal directions, allowing us

to estimate the wetting depth of plastron, following [6], and measure the length of plastron. The boat speed (2-7 m/s) and air saturation level of water (100%-101%) were monitored using a speedometer and a gas sensor, respectively. The surface is flush (step < 30 μm) with the surrounding surface of the boat hull to prevent any possible form drag. The shear stress on the sample surface at different boat speeds was measured using a custom-developed shear sensor, which was reported in [7].

RESULTS

The lengths of the plastron in the longest trench (L_t = 60 mm) were measured, as shown in Figure 3(a), and compared with the theoretical values in Figure 3(b) for different trench pitches and depths. The red shade shows the range of theoretical plastron length for air saturation level of 100%–101%. The lower bound represents an air saturation level of 100%, and the upper represents an air saturation level of 101%. As the speed increases, the shear stress exerted on the plastron by the flowing water increases, decreasing the plastron length. If the maximum plastron length possible for the given trench width and depth is shorter than the given trench, the trench will get wetted; if the maximum plastron length possible for the given trench width and depth is longer than the given trench, the trench will stay dewetted. The experimental results corroborated the developed theory and fit in the theoretical range reasonably well, supporting the combined model to guide the design of SHPo surfaces for future applications.

ACKNOWLEDGEMENTS

The work has been supported by National Science Foundation (NSF) grants 1336966 and 2030404. We appreciate the staff members of the UCLA Nanofabrication Laboratory (NanoLab) for their technical support in fabricating the SHPo samples.

REFERENCES

[1] M, Xu, A. Grabowski, N. Yu, G. Kerezyte, J.-W. Lee, B. R. Pfeifer, C.-J. Kim, "Superhydrophobic Drag Reduction for Turbulent Flows in Open Water", *Phys. Rev. Appl.,* vol. 13, pp. 034056, 2020.

[2] M. Xu, G. Sun, C.-J. Kim, "Infinite lifetime of underwater superhydrophobic states", *Phys. Rev. Lett.,* vol. 113, pp. 136103, 2014.

[3] J. S. Wexler, I. Jacobi, H. A. Stone, "Shear-driven failure of liquid-infused surfaces", *Phys. Rev. Lett.,* vol. 114, pp. 168301, 2015.

[4] F. J. Peaudecerf, J. R. Landel, R. F. Goldstein, P. Luzzatto-Fegiz, "Traces of surfactants can severely limit the drag reduction of superhydrophobic surfaces", *PNAS*, vol. 114, pp. 7254-7259, 2017.

[5] W. Barthlott, T. Schimmel, S. Wiersch, K. Koch, M. Brede, M. Barczewski, S. Walheim, A. Weis, A. Kaltenmaier, A. Leder, H.F. Bohn, "The Salvinia paradox: superhydrophobic surfaces with hydrophilic pins for air retention under water", *Adv. Mater*., vol. 22, pp. 2325-2328, 2010.

[6] N. Yu, S. Kiani, M. Xu, C.-J. Kim, "Brightness of Microtrench Superhydrophobic Surfaces and Visual Detection of Intermediate Wetting States", *Langmuir,* vol. 37, pp. 1206-1214, 2021.

[7] M. Xu, B. Arihara, H. Tong, N. Yu, Y. Ujiie, C.-J. Kim, "A low-profile wall shear comparator to mount and test surface samples", *Exp. Fluids*, vol. 61, pp. 1-13, 2020.

CONTACT

*Ning Yu, tel: +1-310-346-2891; yuning@ucla.edu